Naphthalene dimer: Electronic states, excimers, and triplet decay

Allan L. L. East[a] and Edward C. Lim[b]
Department of Chemistry, The University of Akron, Akron, Ohio 44325-3601

(Received 17 July 2000; accepted 29 August 2000)

Computations have been performed for the singlet and triplet electronic states of varying orientations of naphthalene dimer. The dependence of exciton splitting upon orientation and intermonomer distance was explored. Splittings of triplet states are seen to be nontrivial at typical bonding distances, commensurate with the splittings of weakly allowed singlet states. Charge-transfer interaction with the excimer states is seen to be most significant in face-to-face orientations which can allow closer approach of the two monomers. Predictions of the prominent features of the singlet–singlet and triplet–triplet absorption spectra agree well with experimental findings. A spin-orbit channel-counting scheme is introduced to account for observed radiative and nonradiative decay of the T_1 triplet state of the monomer, and then applied to the dimer. The mechanism has been found for the observed more rapid phosphorescence of the T_1 state of the dimer when placed in orientations lacking inversion symmetry. © *2000 American Institute of Physics.* [S0021-9606(00)00244-0]

I. INTRODUCTION

Intermolecular aromatic–aromatic interactions in the excited states, leading to formation of excimers (dimeric species that are stable only in the excited electronic state), are of fundamental importance in many photochemical reactions. Although much is known about the structure and emission spectrum of singlet excimers, there is still considerable uncertainty about the stability and structure of triplet excimers, and electronic transitions of excimers in general. An improved and detailed understanding of excimers would require relating the electronic states and excitations of dimers to those of the individual chromophores. This particular problem has relevance to photochemical properties of molecular clusters, crystalline solids, polymers, and organized molecular assemblies. Unfortunately, theoretical studies of the electronic states of excimer-forming systems have been very limited in scope. With this paper, we hope to improve this situation substantially in the case of dimers of naphthalene.

Relating the electronic states and excitations of dimers to those of the monomer is primarily a problem of interchromophore interaction. To obtain quantitative energy estimates, however, this relation requires a second step, namely the consideration of several other effects due to the molecular environment. In particular, for dimers that are covalently linked, the linkages can cause chromophore twisting and puckering, as well as electron donating and withdrawing effects. This second step is very system-dependent, and our paper will generally ignore this step in order to concentrate on the more important and more general problem of interchromophore interaction, using unaltered free naphthalene monomers.

Previous theoretical studies of the excited states of two naphthyl units do exist. Scholes and Ghiggino[1] presented a thorough investigation of the energies of the lowest singlet states of the eclipsed dimer, including the effects of intermonomer separation R, based on minimal-basis-set configuration interaction (CIS/STO-3G) calculations. Sadygov and Lim[2] modified a standard semiempirical method (INDO/S) to investigate monomer-orientation dependence of the S_0 and S_1 state energies, and the $S_n \leftarrow S_1$ spectrum of the eclipsed dimer. Gudipati[3] used unmodified INDO/S to compute singlet–singlet excitation energies of various covalently bonded V-shaped naphthalene dimers. Mukamel and co-workers[4] used a specialized method (based on INDO/S) to compute $S_n \leftarrow S_0$ absorption spectra of covalently bonded end-to-end naphthalene dimers, relating them to computed monomer transitions. These and other studies each had a limited focus, and do not go very far at all in addressing the nature of the excited states, the size of the state splittings, and other generally related phenomena.

In this study, we utilize and manipulate the existing INDO/S and CIS quantum chemistry methodologies to more completely elucidate the electronic states and excimers of free dimers of naphthalene. Several different orientations and separations of the monomers are studied, for the interests of wide-ranging applicability to various covalently bonded dimers as well as to the free dimer. The present study provides three significant advances. The first is the set of qualitative and semiquantitative potential energy curves for S_1, T_1, and several other low-lying states of the dimers, for several monomer orientations. The second is the computation of wave functions and energies of up to 60 states, their classification with respect to monomer states, and the associated computation of transition moments and oscillator strengths for S-S and T-T spectra. The third is the discussion of radiative and nonradiative decay of the T_1 state of the dimer, resulting from the use of a new channel-counting technique.

[a]Present address: Department of Chemistry and Biochemistry, University of Regina, Regina, Saskatchewan, S4S 0A2, Canada.
[b]Holder of the Goodyear Chair in Chemistry at The University of Akron, and corresponding author. Electronic Mail: elim@uakron.edu

II. THEORY

A. Excimer theory

Here we wish to summarize many results of excimer theory which are relevant to this work. First we wish to make explicit connections between localized[5] and delocalized[6] excimer theory. Let h and l denote the highest occupied (HOMO) and lowest unoccupied (LUMO) molecular orbitals of monomer A, and h' and l' denote those of monomer B. Then the orbitals of the dimer, at long intermonomer distances, are either equal combinations of h with h', or of l with l', as shown in Fig. 1.

There are four dimer states which arise from the pairing of a ground-state monomer and an excited-state monomer. Chandra and Lim referred to these as σ, γ, δ, and ρ states.[6] These four states can be expressed in terms of localized or delocalized wave functions, depending on whether we choose to perform the single electron excitation in the monomer orbitals or the dimer orbitals of Fig. 1. For the usual case of singlet excited states of eclipsed, sandwichlike dimers, the relevant *delocalized* wave functions (in Slater-determinant notation) are

$$
\begin{aligned}
|\chi_1\rangle &= 2^{-5/2}|(\text{core})(h+h')\underline{(h+h')}[(h-h')\underline{(l+l')} \\
&\quad +(l+l')\underline{(h-h')}]\rangle, \\
|\chi_2\rangle &= 2^{-5/2}|(\text{core})(h+h')\underline{(h+h')}[(h-h')\underline{(l-l')} \\
&\quad +(l-l')\underline{(h-h')}]\rangle, \\
|\chi_3\rangle &= 2^{-5/2}|(\text{core})(h-h')\underline{(h-h')}[(h+h')\underline{(l+l')} \\
&\quad +(l+l')\underline{(h+h')}]\rangle, \\
|\chi_4\rangle &= 2^{-5/2}|(\text{core})(h-h')\underline{(h-h')}[(h+h')\underline{(l-l')} \\
&\quad +(l-l')\underline{(h+h')}]\rangle,
\end{aligned}
\tag{1}
$$

where (core) represents the orbitals of all but the last four electrons, and the absence or presence of an underscore indicates an alpha or beta electron, respectively. The relevant *localized* wave functions are

$$
\begin{aligned}
|A^*B\rangle &= 2^{-1/2}|(\text{core})h'\underline{h'}[h\underline{l}+l\underline{h}]\rangle, \\
|AB^*\rangle &= 2^{-1/2}|(\text{core})h\underline{h}[h'\underline{l'}+l'\underline{h'}]\rangle, \\
|A^-B^+\rangle &= 2^{-1/2}|(\text{core})h\underline{h}[h'\underline{l}+l\underline{h'}]\rangle, \\
|A^+B^-\rangle &= 2^{-1/2}|(\text{core})h'\underline{h'}[h\underline{l'}+l'\underline{h}]\rangle.
\end{aligned}
\tag{2}
$$

At long R values, the above eight wave functions exist in degenerate pairs, so that the true eigenfunctions are the equal mixtures below:

$$
\begin{aligned}
|\sigma\rangle &= 2^{-1/2}(\chi_1+\chi_4) = 2^{-1/2}(A^*B-A^*B), \\
|\gamma\rangle &= 2^{-1/2}(\chi_2+\chi_3) = 2^{-1/2}(A^*B+A^*B), \\
|\delta\rangle &= 2^{-1/2}(\chi_2-\chi_3) = 2^{-1/2}(A^-B^+ + A^+B^-), \\
|\rho\rangle &= 2^{-1/2}(\chi_1-\chi_4) = 2^{-1/2}(A^-B^+ - A^+B^-).
\end{aligned}
\tag{3}
$$

From this correspondence, we see that the σ and γ states are ER (exciton-resonance) states while the δ and ρ states are CT (charge-transfer, or charge-resonance) states.

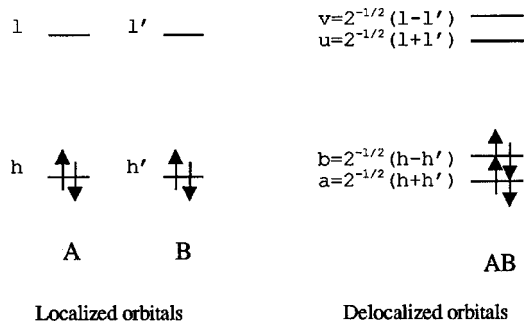

FIG. 1. Molecular orbitals in the localized and delocalized excimer theories.

The energy expressions for these four states can be derived using delocalized theory and then converted to monomer orbital notation. The results for relative energies from the ground-state E_0 are expressed below for both singlet and triplet excitations:

$$
\begin{aligned}
E(^1\sigma)-E_0 &= \Delta E - J_{hl} + 2K_{hl} - 2K'_{hl'}, \\
E(^1\gamma)-E_0 &= \Delta E - J_{hl} + 2K_{hl} + 2K'_{hl'}, \\
E(^1\delta)-E_0 &= \Delta E - J_{hl'}, \\
E(^1\rho)-E_0 &= \Delta E - J_{hl'}, \\
E(^3\sigma)-E_0 &= \Delta E - J_{hl}, \\
E(^3\gamma)-E_0 &= \Delta E - J_{hl}, \\
E(^3\delta)-E_0 &= \Delta E - J_{hl'}, \\
E(^3\rho)-E_0 &= \Delta E - J_{hl'}.
\end{aligned}
\tag{4}
$$

Here ΔE is the orbital energy difference $(\epsilon_v+\epsilon_u-\epsilon_b-\epsilon_a)/2$, and the two-electron integrals are $J_{hl}=(hh|ll)$, $K_{hl}=(hl|hl)$, $J_{hl'}=(hh|l'l')$, and $K'_{hl'}=(hl|h'l')$. Hence, at long R values, the four charge-transfer states should have the same energy, and an excimer splitting (exciton splitting) exists between the $^1\sigma$ and $^1\gamma$ states, but not between the $^3\sigma$ and $^3\gamma$ states. The $J_{hl'}$ and $K'_{hl'}$ terms are R-dependent, resulting in a significant attractive potential for the CT states and the R-dependent excimer splitting. The excimer splitting of $4K'_{hl'}$ has also been approximated[5] as $\mathbf{M}_A\cdot\mathbf{M}_B/R^3$, where $\mathbf{M}_A$ and $\mathbf{M}_B$ are the transition moment vectors of local excitations on monomer A or B, respectively.

For didactic purposes, we performed CIS calculations (see Sec. III) of these eight states for the D_{2h}-symmetry face-to-face approach of two ethene molecules, with the results plotted in Fig. 2. In this case, computed values for the constant terms ΔE, J_{hl}, and K_{hl} are 15, 11, and 2.5 eV, respectively, and the qualitative features are as predicted at large R values. At $R<5$ Å, however, orbital–orbital and state–state interactions affect results, most notably the coupling between the ρ CT and σ ER states. Scholes and Ghiggino,[1] in their discussion of interchromophore interactions, referred to two different interaction regions which they called short-range (3–6 Å) and intermediate-range (6–150 Å), and showed that the basic excimer-theory results hold only in the

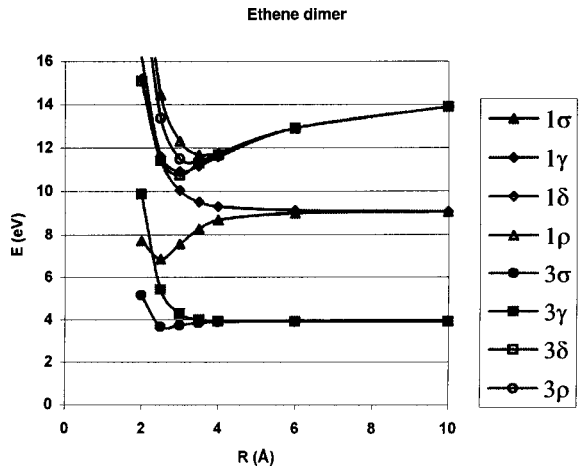

FIG. 2. A plot of the eight states of C_2H_4 dimer which arise from $\pi\rightarrow\pi^*$ excitation, as computed from CIS/6-31G. Only the $(^1\sigma,^1\gamma)$ state pair show noticeable splitting at $R>5$ Å.

intermediate-range. Our Fig. 2 demonstrates this as well. Hence, excimer-theory results for the excimer splitting ($4K'_{hl}$ or $\mathbf{M}_A\cdot\mathbf{M}_B/R^3$) should *not* be expected to hold in dimer-bonding regions of alkenes or planar aromatic systems.

B. $S_0\leftarrow T_1$ transition theory

Radiative T_1 decay (phosphorescence) is forbidden under the usual nonrelativistic Born–Oppenheimer approximation. The decay rate is proportional to the square of the transition moment $\langle S_0|M|T_1\rangle$. Expressions for the forbidden transition moment can be obtained using perturbation theory, where the perturbing Hamiltonian is the spin-orbit Hamiltonian H_{SO}. The result is

$$\begin{aligned}\langle S_0|M|T_1\rangle &= [\langle T_1|M|T_1\rangle-\langle S_0|M|S_0\rangle]\langle S_0|H_{\mathrm{SO}}|T_1\rangle/[E(S_0)-E(T_1)]\\ &\quad+\Sigma_{Sn}\{\langle S_0|M|S_n\rangle\langle S_n|H_{\mathrm{SO}}|T_1\rangle/[E(T_1)-E(S_n)]\}\\ &\quad+\Sigma_{Tn}\{\langle T_1|M|T_n\rangle\langle T_n|H_{\mathrm{SO}}|S_0\rangle/[E(S_0)-E(T_n)]\},\end{aligned}\tag{5}$$

where the first term is a dipole moment difference term, the second term represents borrowing of intensity from singlet–singlet transitions, and the third term represents borrowing from triplet–triplet transitions. Note that $|T_1\rangle$ has three components, each of which has its own individual decay rate and polarization direction.

Nonradiative T_1 decay can be treated using time-dependent perturbation theory. Its so-called Golden Rule[7] expresses this decay rate as proportional to the square of the expectation value $H'_{01}=\langle S_0|T_{\mathrm{nuc}}+H_{\mathrm{SO}}|T_1\rangle$, where T_{nuc} is the nuclear kinetic energy operator and $\langle S_0|$ and $|T_1\rangle$ are eigenfunctions of the full Hamiltonian (including T_{nuc} and H_{SO}). Expressions for H'_{01} can be obtained using regular perturbation theory, where the perturbing Hamiltonian is only the spin-orbit Hamiltonian H_{SO}, as in the radiative transition case. Henry and Siebrand[8] applied several simplifying approximations, and their result is

$$\begin{aligned}H'_{01}&=F_{01}\langle S_0|H_{\mathrm{SO}}|T_1\rangle\\ &\quad+F_{01}\Sigma_{Qk}\Sigma_{Sn}\{(C^-_{nk})^*\langle S_0|\partial/\partial Q_k|S_n\rangle^*\langle S_n|H_{\mathrm{SO}}|T_1\rangle\}\\ &\quad+F_{01}\Sigma_{Qk}\Sigma_{Tn}\{(C^+_{nk})^*\langle T_1|\partial/\partial Q_k|T_n\rangle^*\langle T_n|H_{\mathrm{SO}}|S_0\rangle\},\end{aligned}\tag{6}$$

where F_{01} is the Franck–Condon factor, k is a normal mode index, n is an electronic state index, $\partial/\partial Q_k$ is the derivative with respect to normal mode Q_k, and C^-_{nk} and C^+_{nk} are Q_k-dependent coefficients which also include the electronic energy difference denominators $E(T_1)-E(S_n)$ and $E(S_0)-E(T_n)$. We shall drop the F_{01} factor, as we did for Eq. (5). A further approximation would be to neglect Henry and Siebrand's mechanism #2 (from Herzberg–Teller expansion), in which case the result is

$$\begin{aligned}H'_{01}&=\langle S_0|H_{\mathrm{SO}}|T_1\rangle\\ &\quad+\Sigma_{Qk}\Sigma_{Sn}\{C_k\langle S_0|\partial/\partial Q_k|S_n\rangle^*\langle S_n|H_{\mathrm{SO}}|T_1\rangle/[E(T_1)-E(S_n)]\}\\ &\quad+\Sigma_{Qk}\Sigma_{Tn}\{C_k\langle T_1|\partial/\partial Q_k|T_n\rangle^*\langle T_n|H_{\mathrm{SO}}|S_0\rangle/\\ &\quad[E(S_0)-E(T_n)]\},\end{aligned}\tag{7}$$

where C_k is a Q_k-dependent term with no dependence upon electronic energy. Note again that $|T_1\rangle$ has three components, each of which has its own individual decay rate.

Both the radiative and nonradiative decay rates can thus be expressed as proportional to the square of an expectation value W_{01}, this value having the form

$$\begin{aligned}W_{01}&=A_{01}\langle S_0|H_{\mathrm{SO}}|T_1\rangle+\Sigma_{Sn}A_{Sn}\langle S_n|H_{\mathrm{SO}}|T_1\rangle\\ &\quad+\Sigma_{Tn}A_{Tn}\langle T_n|H_{\mathrm{SO}}|S_0\rangle.\end{aligned}\tag{8}$$

Equation (8) is written in terms of *spin-orbit channels*. For some molecules, the excited-state sums are dominated by one or two low-lying spin-orbit channels, and only a few terms in the sum are needed for reasonable results. Unfortunately, one could very well ask whether this is the exception or the rule. For many molecules with relatively long T_1 lifetimes, such as naphthalene, there are no low-lying channels that dominate, and the summations over excited states converge very slowly. Even with molecules having lone pairs of electrons, which have significant low-lying channels, one cannot always get away with considering only the lowest-lying S_n or T_n states. Langhoff and Davidson,[9] for instance, performed calculations for the phosphorescence of H_2CO many years ago, and obtained significant variation in lifetimes depending on whether they considered only 12 excited states or 100 of them.

We introduce here a simple *channel-counting scheme* which seems to work for naphthalene monomer, and which may have general applicability for molecules for which the above excited-state summations converge slowly. First, using molecular orbital theory, we count all possible spin-orbit channels, via various S_n and T_n states other than Rydberg or core-excitation states. H_{SO} is a one-electron operator, and hence can only connect states that differ by one orbital occupation. In addition, it has only three spatial-symmetry

TABLE I. Naphthalene monomer: computed ($S_n \leftarrow S_0$) absorption spectrum.[a]

State[b]	Symmetry[c]	INDO/S	CIS/6-31G	CIS/6-31+G	CASPT2F[d]
$S^{01+}(^1L_b)$	$^1B_{2u}$	S_1 3.8 (0.01)	S_2 5.4 (0.0001)	S_2 5.3 (0.003)	4.03(0.0004)
$S^{00}(^1L_a)$	$^1B_{1u}$	S_2 4.3 (0.22)	S_1 5.1 (0.16)	S_1 5.0 (0.16)	4.56(0.05)
$S^{01-}(^1B_b)$	$^1B_{2u}$	S_4 5.5 (1.79)	S_4 7.4 (2.46)	S_8 6.9 (2.01)	5.54(1.34)
S^{11}	$^1B_{1u}$	S_7 6.1 (0.55)	S_5 7.7 (0.59)	S_{15} 7.4 (0.63)	5.93(0.31)
$S(h_{-1}\rightarrow 3s)$	$^1B_{3u}$	⋯	⋯	S_{12} 7.4 (0.01)	6.03(0.003)
$S(h_0\rightarrow 3d_1)$	$^1B_{3u}$	⋯	⋯	S_7 6.8 (0.06)	6.50(0.007)
$S(h_0\rightarrow 3d_2)$	$^1B_{1u}$	⋯	⋯	S_{21} 8.0 (0.02)	6.67(0.002)
$S(h_0\rightarrow 3d_3)$	$^1B_{2u}$	⋯	⋯	S_{17} 7.7 (0.46)	6.85(0.018)
S^{22}	$^1B_{1u}$	S_{23} 7.7 (0.66)	S_{21} 10.2 (0.83)	S_{40} 9.2 (0.57)	7.16(0.85)

[a]Table entries: state number S_n, vertical excitation energies in eV, and (in parentheses) oscillator strength f values. Transitions to the $^3B_{1u}$, $^3B_{2u}$ and $^3B_{3u}$ states are polarized along the short, long, and out-of-plane axes, respectively.

[b]Upper $\pi\rightarrow\pi^*$ states S^{ij} are characterized according to the orbital excitations $\phi_{-i}\rightarrow\phi_j$ of the leading term in the wavefunction (see text for details), with Platt notation in parentheses. Upper Rydberg states are labeled by the explicit orbital excitation involved.

[c]State symmetries, using the Mulliken (not Pariser) symmetry convention, i.e., the short and long axes are *z* and *y*, respectively.

[d]From Rubio *et al.* (Ref. 15).

components for singlet-triplet coupling (B_{1g}, B_{2g}, B_{3g} for D_{2h} systems) which will restrict the number of allowed spin-orbit channels.

Second, we come up with estimates for the typical values of the spin-orbit-coupling magnitudes and the A coefficients in Eq. (8), considering different values for different types of excited states. These come from either *ab initio* calculation or best guesses. Third, the W_{01} values are then computed for each T_1 component, and the results are squared and averaged to mimic T_1 decay rates. This procedure is demonstrated in Sec. IV E for naphthalene monomer.

III. COMPUTATIONAL METHODS

The calculations were performed with GAUSSIAN98.[10] Electronic state wave functions and energies were computed with two methods: the intermediate neglect of differential overlap method for spectroscopy (INDO/S)[11] (called ZINDO in GAUSSIAN98) and regular configuration interaction (CIS).[12] Both methods consider only single excitations from the reference configuration. The active spaces for the CIS excitations encompassed all orbitals except the core ones, while for INDO/S we activated 10 occupies and 10 virtuals for naphthalene monomer and 20-and-20 for the dimer.

The INDO/S method is not parametrized for bichromophore interactions, and produced a catastrophic failure for $R<$about 3.6 or 3.7 Å, at which all potential curves become extremely and unphysically attractive in every orientation. Hence, for the generation of excited state *E*-versus-*R* curves for a wide range of *R* values, INDO/S is inappropriate, and we had to resort to an *ab initio* method which could handle a 20-carbon system, namely CIS. For the spectral tables, where we were more concerned with state ordering and intensity rather than transition energy, we used INDO/S at 3.6 Å or above.

For a gauge of dynamical correlation in Sec. IV B below, we used Møller–Plesset perturbation theory (MP2).[13]

For spin-orbit coupling calculations, we used the state-averaged determinant-based complete-active-space self-consistent field (CASSCF) technique of Gordon and co-workers.[10,14] The state-averaging weights were given equally to only the S_0 and T_1 states, regardless of the states selected for the spin-orbit coupling integral. For naphthalene dimer, we used the largest active space we could, which was 8 electrons in 8 orbitals (giving 4900 determinants); fortunately the results seemed quite consistent when smaller active spaces (4-in-6 and 8-in-6) were tested. Active spaces for the monomer calculations varied from 2-in-5 to 8-in-5, depending on the intermediate state involved. The active spaces for the other systems in Sec. IV F were: 4-in-6 for ethene dimer, and 8-in-6 for the covalently bound dinaphthyl compounds.

The size of the system necessitated the use of a limited basis set, particularly for the CASSCF calculations, and we generally chose the 6-31G set (212 basis functions for naphthalene dimer).[10] The monomer geometries were held fixed ($R_{CC}=1.406$ Å, $R_{CH}=1.08$ Å) throughout the study.

IV. RESULTS AND DISCUSSION

A. Review of monomer $S_n\leftarrow S_0$ and $T_n\leftarrow T_1$ spectra

The best summary of the singlet–singlet ($S_n\leftarrow S_0$) and triplet–triplet ($T_n\leftarrow T_1$) electronic spectra of naphthalene appears in the 1994 paper of Rubio *et al.*,[15] who reproduced the observed spectra with line positions of 0.5 eV accuracy using *ab initio* methods (CASPT2 for energies and CASSI for transition moments). Very good results for the *S*-*S* spectrum were also obtained by Bak *et al.*, using SOPPA, another *ab initio* method.[16] Briefly, the experimental *S*-*S* spectra exhibit strong and broad electronic transitions at wavelengths near 220, 205, and 165 nm, respectively, with the 205 nm band appearing as a shoulder of the more substantial 220 nm band. The lowest-lying S_1 and S_2 states, denoted ^1L_b and ^1L_a in Platt's notation, weakly absorb near 310 and 275 nm, respectively. The experimental *T*-*T* spectra show a few weak bands but only one of medium intensity, near 400 nm, although we predict another to exist in the 200–250 nm range.

Table I compares the monomer *S*-*S* spectrum results of some simpler methods (INDO/S, CIS/6-31G, CIS/6-31+G)

TABLE II. Naphthalene monomer: computed ($T_n \leftarrow T_1$) absorption spectrum.[a]

Label[b]	Symmetry[c]	INDO/S	CIS/6-31G	CIS/6-31+G	CASPT2F[d]
T^{00}	$^3B_{1u}$	[1.4 above S_0]	[2.2 above S_0]	[2.3 above S_0]	[3.04 above S_0]
T^{01+e}	$^3B_{2u}$	T_3 1.7 (0.000)	T_3 2.1 (0.000)	T_3 2.0 (0.000)	0.80 (0.000)
T^{02+}	$^3B_{3g}$	T_2 1.1 (0.001)	T_2 1.6 (10^{-5})	T_2 1.7 (10^{-4})	1.14 (10^{-5})
T^{03+}	^3A_g	T_5 2.3 (0.007)	T_6 3.2 (0.001)	T_6 3.1 (0.001)	2.18 (0.001)
T^{02-}	$^3B_{3g}$	T_{11} 4.3 (0.395)	T_{10} 5.7 (0.543)	T_{21} 5.5 (0.319)	2.61 (0.097)
T^{12-}	^3A_g	T_{12} 4.4 (0.014)	T_9 5.4 (0.036)	T_{19} 5.2 (0.035)	2.73 (10^{-6})
T^{12+}	^3A_g	T_8 3.6 (0.017)	T_8 5.2 (0.007)	T_{14} 4.7 (0.004)	2.81 (0.001)
T^{31}	$^3B_{3g}$	T_7 3.5 (0.001)	T_7 5.1 (0.012)	T_{15} 4.9 (0.073)	3.14 (0.001)
T^{03-}	^3A_g	T_{23} 5.7 (0.343)	T_{27} 8.1 (0.587)	T_{36} 6.4 (0.018)	⋯

[a]Table entries: state number T_n, vertical excitation energies in eV, and (in parentheses) oscillator strength f values. Transitions to the ^3A_g, $^3B_{3g}$ and $^3B_{2g}$ states are polarized along the short, long, and out-of-plane axes, respectively.

[b]Upper $\pi \rightarrow \pi^*$ states T^{ij} are characterized according to the orbital excitations $\mathscr{h}_{-i} \rightarrow \mathscr{l}_j$ of the leading term in the wavefunction (see text for details).

[c]State symmetries, using the Mulliken (not Pariser) symmetry convention, i.e., the short and long axes are z and y, respectively.

[d]From Rubio *et al.* (Ref. 15).

[e]The forbidden T^{01+} state is included here for reference purposes only.

against the CASPT2 results of Rubio *et al.*[15] Table II does the same for the T-T spectrum. The state labels S^{ij} (or T^{ij}) refer to the orbital excitation ($\mathscr{h}_{-i} \rightarrow \mathscr{l}_j$) which principally characterizes the excited state in molecular orbital theory; the five π and five π^* orbitals are labeled (in increasing order of energy) $\mathscr{h}_{-4}$, $\mathscr{h}_{-3}$, $\mathscr{h}_{-2}$, $\mathscr{h}_{-1}$, $\mathscr{h}_0$, $\mathscr{l}_0$, $\mathscr{l}_1$, $\mathscr{l}_2$, $\mathscr{l}_3$, $\mathscr{l}_4$. A superscripted sign indicates that the state is a roughly equal mixture of the ($\mathscr{h}_{-i} \rightarrow \mathscr{l}_j$) and ($\mathscr{h}_{-j} \rightarrow \mathscr{l}_i$) excitations, combined with the specified phase. The S_n and T_n state-counting labels, particularly those of the CIS/6-31+G columns (which account for Rydberg states as well), will give the reader a rough idea of the number of nonabsorbing or weakly absorbing states omitted from these tabulations. Note, however, that the INDO/S and CIS methods will not account for the (generally invisible) states arising from double or greater excitations.

In Table I, the INDO/S results are seen to be in fortuitously good agreement with the more reliable CASPT2 results, demonstrating 0.3 eV agreement for the pertinent states below 7 eV. The CIS results are poorer, overestimating the excitation energies and inverting the order of the first two excited states. The oscillator strengths, listed in parentheses, are in rough accord across the table, with the INDO/S and CIS intensities being somewhat too large as usual.[17] In Table II, the INDO/S energies are shown to be less accurate for the T-T spectrum, although not as bad as the CIS energies. The agreement amongst oscillator strength computations here is still qualitative, but not as quantitative as in the S-S spectrum.

These tables will serve as reference guides for the dimer state studies below.

B. Diagrams of *E* vs. *R* for various dimer orientations

The preferred orientation of the naphthalene monomers in the free dimer is known definitively only for the singlet excimer states, in which the monomers are in an eclipsed, sandwichlike conformation.[18] For the triplet state, an L-shaped orientation has been hypothesized,[19,20] although this remains unverified. The ground-state dimer may not have a well-defined orientation at all, since recent MP2 calculations placed four conformations within 1.3 kcal/mol of each other in energy[21] and the best computations of the more-often-studied benzene dimer now imply a fluxional system with several low-frequency modes.[22–24] In addition to the orientation problem, the dependence of state splittings upon intermonomer distance R varies considerably with the nature of the monomer-state, and there is a long-standing need to determine such dependencies and provide qualitative and semiquantitative energy curve diagrams for common chromophore dimers. We hence undertook an examination of the energies of dozens of singlet and triplet states of the dimer of naphthalene, as functions of intermonomer distance R, for several different monomer orientations.

We chose to study five particular orientations: eclipsed (D_{2h}), 10°-conrotated (parallel-displaced, C_{2h}), 45°-disrotated (L-shaped, C_{2v}), T-shaped (C_{2v}), and crossed (D_{2d}). The T- and L-shaped orientations are so-called because the short axes of their monomers form a ''T'' or right angle, respectively. These orientations appear in Fig. 3. The results of the conrotated dimer were very similar to those of the eclipsed, however, and are not considered any further.

The electronic state energies were initially computed with CIS/6-31G, but required several corrections in order to arrive at qualitative and semiquantitative results. First, CIS does not account for dynamical electron correlation, and hence resulted in almost all states being repulsive. Second, CIS gives poor energy orderings for the monomer states,

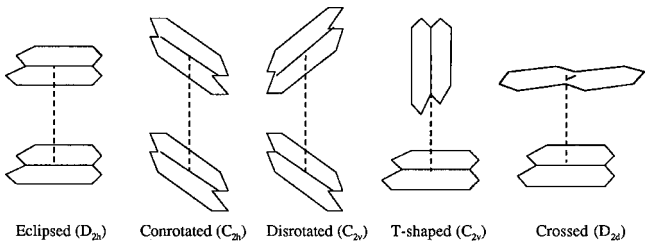

FIG. 3. Five hypothetical orientations of the naphthalene dimer.

which results in poor orderings for the dimer states. Third, significant couplings between exciton-resonance and corresponding charge-transfer states were underestimated due to the poor CIS monomer energies, resulting in occasional noticeable errors in excitation energies.

For the first problem, all curves were corrected with a $-C/R^6$ orientation-dependent correlation correction.[22] This orientation-dependent $-C/R^6$ correction was derived from ground-state MP2/6-31G energies computed at two values of R, and applied equally to each state, using the crude assumption that the state-dependence of the dispersive attraction of the two monomers will be negligible on the scale of our plots.

For the second problem, all σ- and γ-state curves were given constant shifts so that their respective dissociation asymptotes matched the more accurate CASPT2 monomer energies.[15] In addition, the δ^{00}-state and ρ^{00}-state CT curves were given a constant shift so that their dissociation limit matched the experimental ionization energy of the monomer (65 690 cm^{-1}),[25] since these states correlate to the cation and autoionized anion ($C_{10}H_8^+ + C_{10}H_8 + e^-$).

For the third problem, we used a more intricate procedure to correct the coupling between ER and CT states. We performed this correction only for σ^{00}-ρ^{00} interactions (for all four orientations) and γ^{00}-δ^{00} interactions (for all except the eclipsed orientation), these being the only ones which significantly affected the states of interest. The correction incorporates the asymptote shifts of the preceding paragraph, and involved the following steps:

(1) The two decoupled (diabatic) states were derived from the data, using the observed CI coefficients.

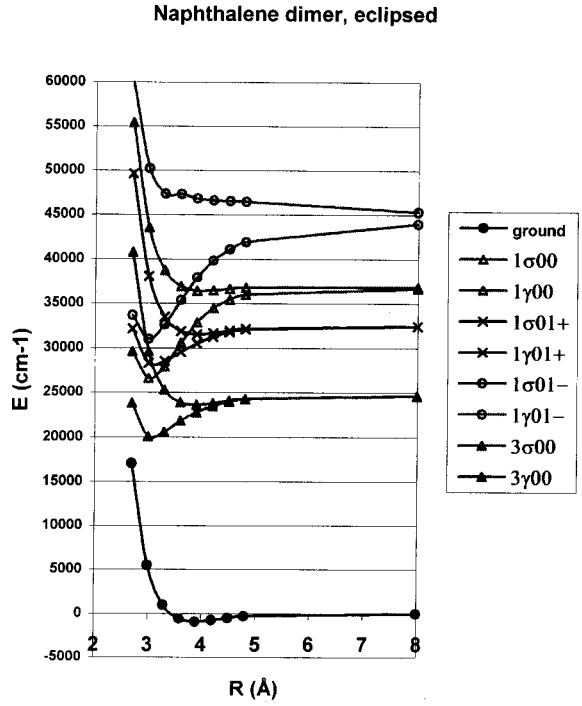

FIG. 4. Eclipsed naphthalene dimer. Energies (in cm^{-1}) of the ground state, and the σ and γ products of the monomer ^3L_a, ^1L_b, ^1L_a, and ^1B_b states, as functions of intermonomer separation.

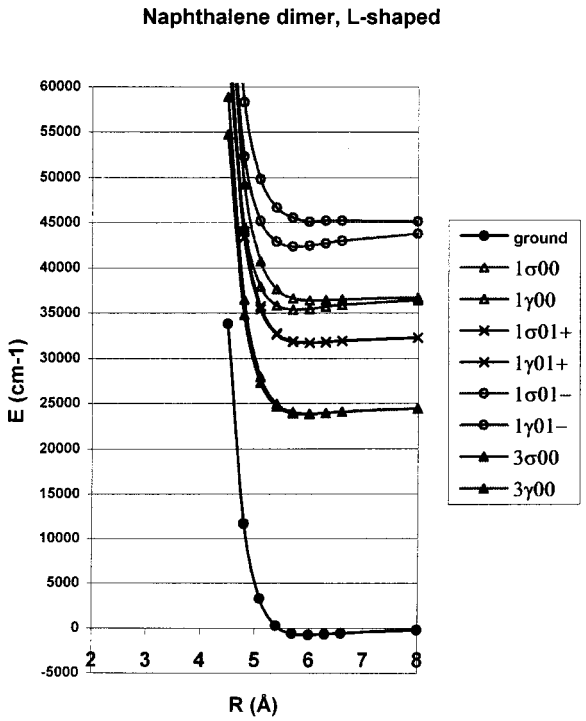

FIG. 5. L-shaped naphthalene dimer. Energies (in cm^{-1}) of the ground state, and the σ and γ products of the monomer ^3L_a, ^1L_b, ^1L_a, and ^1B_b states, as functions of intermonomer separation.

(2) The interaction matrix element, a function of the orbitals but not the energy gap, was derived from the data.
(3) The two decoupled states were given constant shifts to give correct dissociation asymptotes.
(4) The two states were recoupled using the interaction matrix element of step-2.

The effects of the decoupling and recoupling in steps (1) and (4) were divided equally among the two states. For the T-shaped dimer, step (1) was more complicated because each molecular orbital showed a partial preference for one monomer or the other, and hence its formula for the fraction of the diabatic CT state in the adiabatic lower-state wave function involved the LCAO-MO coefficients as well as the CI ones.

We also considered corrections for two other possible weaknesses: the small 6-31G basis set and basis set superposition error (BSSE). We investigated possible improvements on MP2/6-31G energies using the larger 6-311G$(2d,p)$ basis set and the counterpoise correction,[26] respectively, and although both effects were on the order of 500–1700 cm^{-1} at ground-state geometries, they in fact cancelled each other to within 500 cm^{-1}. A similar observation was made by Jaffe and Smith for benzene dimer.[22] Hence, we made no further corrections to the data.

Figures 4 through 7 show the results for the ground state and the σ and γ combinations of the ^3L_a, ^1L_b, ^1L_a, and ^1B_b states of naphthalene. These figures are, to our knowledge, the first qualitatively accurate plots of the R-dependence of these states in any orientation. We will mention three possible theoretical weaknesses in these curves. One is that the CIS splittings may be a bit too large, as seen in our calculations on 1,3-diphenylpropane.[27] Another is that the expected

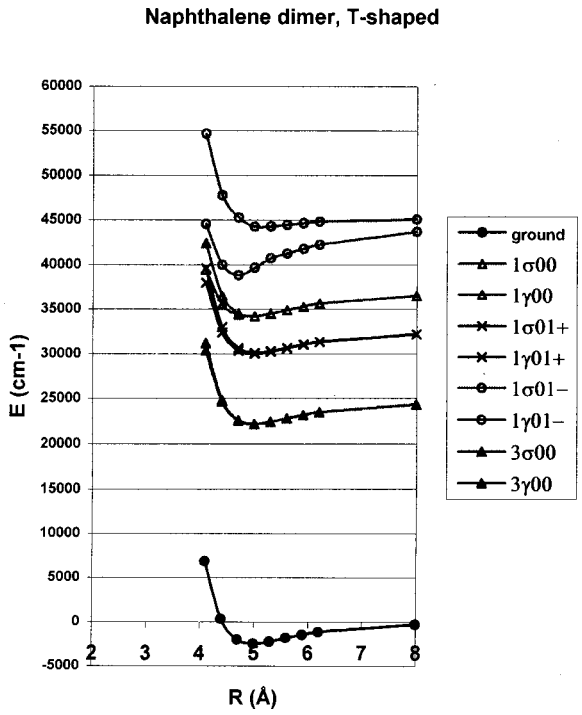

FIG. 6. T-shaped naphthalene dimer. Energies (in cm^{-1}) of the ground state, and the σ and γ products of the monomer ^3L_a, ^1L_b, ^1L_a, and ^1B_b states, as functions of intermonomer separation.

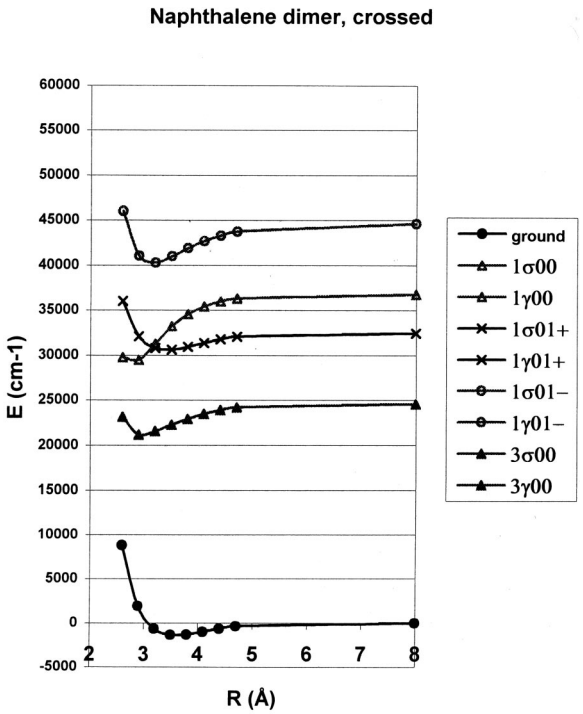

FIG. 7. Crossed naphthalene dimer. Energies (in cm^{-1}) of the ground state, and the σ and γ products of the monomer ^3L_a, ^1L_b, ^1L_a, and ^1B_b states, as functions of intermonomer separation.

accuracy of the predicted binding energies is only about 2000 cm^{-1}, which prevents our use of these figures alone to make conclusions on the preferred orientations of various states. A third weakness is that the calculations, based on ground-state orbitals, do not allow for the differences in spatial extent that is known to exist between the electron densities of a triplet state and its corresponding open-shell singlet state. With the caveats stated, we now proceed to discuss these figures.

For $R>5$ Å (6 Å for the T- and L-shaped orientations), CT state interaction and orbital overlap effects are minimal, and the observed splittings are excimeric in nature. For the eclipsed dimer, a large excimer splitting is seen for the bright, long-axis-polarized ^1B_b (S^{01+}) state, a smaller splitting for the short-axis-polarized ^1L_a (S^{00}) state, and very little splitting for the long-axis-polarized ^1L_b (S^{01-}) state. For the crossed dimer, excimer splittings disappear because the monomer transition moments $\mathbf{M}_A$ and $\mathbf{M}_B$ are perpendicular, and hence the dot product in the $\mathbf{M}_A \cdot \mathbf{M}_B / R^3$ rule is zero. The excimer splitting of the ^1L_a state was expected to disappear for the T- and L-shaped orientations also, since the short axes of the monomers are perpendicular in these cases also, but an excimer splitting is seen for the L-shaped orientation. This we attribute to rotation of $\mathbf{M}_A$ and $\mathbf{M}_B$ due to the presence of the other monomer in an asymmetrical position. The triplet σ^{00} and γ^{00} states show no excimer splitting in any orientation.

In bonding regions, however, CT interaction and other effects are significant, and in some cases are the *leading* contributors to state stability. CT interaction is the strongest for the eclipsed and crossed orientations, which can afford a very close approach of the two monomers. CT interaction is one of the reasons (the other being the excitation resonance) for the $^1\sigma^{00}$ state being the lowest singlet excited state of these two orientations, despite the fact that its parent S^{00} state is only the second-lowest excited state in the monomer. It is also the reason for the surprisingly bound wells in the triplet states of these two orientations, and for the $^3\sigma^{00}$-$^3\gamma^{00}$ splitting being as large as that of $^1\sigma^{01+}$-$^1\gamma^{01+}$. The CT interaction effect is weak for the T-shaped orientation, despite the existence of an additional feature: in this orientation the monomers are inequivalent, which forces the δ^{00} and ρ^{00} CT states to mix and creates a CT state which lies lower than usual.

We suspect that the true T_1 states are not as well bound as they appear in the eclipsed and crossed orientations, with the problem lying possibly in the use of ground-state orbitals, or the use of a common MP2 correction. If this binding is indeed too enhanced, then the triplet excimer may exist in several different orientations, or even be rather fluxional in nature.

These calculated figures offer predictions for all kinds of excimer properties, from preferred R values to expected wavelengths of absorption, fluorescence, and phosphorescence.

C. Analysis of dimer $S_n \leftarrow S_0$ spectra

For modeling of the absorption or fluorescence excitation spectrum of naphthalene dimer, we used the INDO/S method for intensity reliability. Table III shows our INDO/S results for several singlet states of the dimer, at the eclipsed (sandwich) and 20°-disrotated (V-shaped) orientations, at in-

TABLE III. Naphthalene dimer: computed ($S_n \leftarrow S_0$) absorption spectrum.[a]

Monomer		Dimer		Eclipsed dimer, $R=3.8$ Å				V-shaped dimer, $R=4.4$ Å			
S_n	E(eV)	f	State label	S_n	E(eV)	f	**M** vector (a.u.)	S_n	E(eV)	f	**M** vector (a.u.)
$S_1(S^{01+})$	3.85	0.01	σ_1	S_1	3.76	⋯	⋯	S_1	3.81	⋯	⋯
			γ_1	S_2	3.84	0.01	0.30,x	S_2	3.84	0.01	0.35,x
			δ_1	S_{11}	5.45	0.65	2.20,x	S_{12}	5.58	1.71	3.53,x
			ρ_1	S_{13}	5.62	⋯	⋯	S_{13}	5.75	⋯	⋯
$S_2(S^{00})$	4.27	0.22	σ_2	S_3	3.99	⋯	⋯	S_3	4.06	0.08	0.88,y
			γ_2	S_4	4.28	0.33	1.78,z	S_4	4.29	0.32	1.75,z
			δ_2	S_5	4.73	0.02	0.46,z	S_5	4.85	0.01	0.27,z
			ρ_2	S_6	4.90	⋯	⋯	S_6	5.00	0.00	0.16,y
S_3	5.40	⋯	σ_3	S_8	5.28	⋯	⋯	S_8	5.31	⋯	⋯
			γ_3	S_9	5.38	⋯	⋯	S_9	5.39	0.01	0.27,x
$S_4(S^{01-})$	5.48	1.79	σ_4	S_7	4.95	⋯	⋯	S_7	5.16	⋯	⋯
			γ_4	S_{18}	5.88	2.12	3.84,x	S_{15}	5.79	1.79	3.55,x
			δ_4	S_{14}	5.63	0.77	2.36,x	S_{17}	5.89	0.02	0.37,x
			ρ_4	S_{19}	5.92	⋯	⋯	S_{18}	5.94	⋯	⋯
S_5	5.51	⋯	σ_5	S_{10}	5.41	0.00	0.01,y	S_{10}	5.47	0.00	0.01,y
			γ_5	S_{12}	5.47	⋯	⋯	S_{11}	5.50	0.00	0.02,z
S_6	5.82	⋯	σ_6	S_{16}	5.78	⋯	⋯	S_{14}	5.78	⋯	⋯
			γ_6	S_{17}	5.78	0.00	0.02,x	S_{16}	5.79	0.01	0.23,x
$S_7(S^{11})$	6.07	0.55	σ_7	S_{15}	5.75	⋯	⋯	S_{19}	5.97	0.13	0.95,y
			γ_7	S_{21}	6.07	0.85	2.39,z	S_{21}	6.14	0.90	2.44,z
			δ_7	S_{29}	6.59	0.16	0.98,z	S_{33}	6.72	0.01	0.20,z
			ρ_7	S_{34}	6.71	⋯	⋯	S_{34}	6.74	0.00	0.01,y
$S_{23}(S^{22})$	7.73	0.66	σ_{23}	S_{57}	7.46	⋯	⋯	S_{56}	7.51	0.13	0.83,y
			γ_{23}	S_{65}	7.71	1.31	2.64,z	S_{62}	7.73	0.77	2.02,z

[a]All results, including S_n numbering, are from INDO/S calculations. The oscillator strength f is for the transition from the ground (S_0) state. Transition moment directions are given by axis, where x is the long axis of each monomer and y is the intermonomer axis.

termonomer distances thought to be plausible for the S_0 state based on Figs. 4 and 5. The V-shaped orientation data are included here for the later discussion of dimer phosphorescence, and also provide a demonstration of the effect of one particular orientation displacement. The dimer states are labeled according to the notation of Sec. II A; for each monomer state S_n there corresponds the four states σ_n, γ_n, δ_n, and ρ_n, with the latter two denoting the states of predominantly charge-transfer character. The table is arranged in such a way as to see how the intensity in the dimer spectrum arises from the intensity in the monomer spectrum. Note that the S_n labels are numbered according to INDO/S ordering and will not exactly correspond to the true state ordering.

For $S_n \leftarrow S_0$ monomer transitions which are long-axis-polarized ($S_1, S_4, \ldots$) or short-axis polarized ($S_2, S_7, \ldots$), the dimer $S_n \leftarrow S_0$ transitions to the σ and ρ states are forbidden for eclipsed or conrotated (parallel-displaced) geometries. This means that in the dimer orientations thought to prevail for singlet excimers or the ground state, $S_1 - S_0$ transitions are *very weak*. For disrotated (V-shaped) dimers, the same situation occurs for the long-axis-polarized transitions, but for the short-axis-polarized ones the four corresponding states will all provide allowed transitions.

Normally the excimer splitting (between σ and γ states) is far smaller than the gap between the excimer and charge-transfer states. However, for the S_4 monomer state, INDO/S gives an excimer splitting of roughly 1 eV, placing the strongly allowed γ_4 state in the vicinity of the δ_4 state, lending intensity to it as well as to the δ_1 state.

Hence, the most substantial changes to the naphthalene $S_n \leftarrow S_0$ absorption spectrum upon dimerization should be the varying blue shifts of S_n to γ_n, with two charge-transfer bands appearing between 5.5 and 6 eV.

D. Analysis of dimer $T_n \leftarrow T_1$ and $S_n \leftarrow S_1$ spectra

Table IV shows our INDO/S results for several triplet states of the dimer, again at the eclipsed and 20°-disrotated orientations, at slightly smaller intermonomer distances than those used in Table III. While our Fig. 4 suggests that the T_1 state prefers even smaller values of R, we are reluctant to use INDO/S for such values (see Sec. III). This table is arranged similarly to that of Table III, but with energies E and oscillator strengths f corresponding to $T_n \leftarrow T_1$ transitions. Note that the absolute transition energies are *poor predictions in this case*, because of INDO/S inaccuracy for triplet state energies, as we demonstrated for the monomer in Table II. However, the σ-γ and δ-ρ splittings should be unaffected by these absolute errors.

For $T_n \leftarrow T_1$ monomer transitions which are long-axis-polarized ($T_2, T_{11}, \ldots$) or short-axis polarized ($T_5, T_8, \ldots$), the dimer $T_n \leftarrow T_1$ transitions to the γ and δ states are forbidden for eclipsed or conrotated geometries. This is opposite to the rule for $S_n - S_0$ transitions, caused by the fact that the lower state of transition here is already a σ state. For disrotated dimers, the four states corresponding to each short-axis-polarized transition are all allowed, just as for the $S_n - S_0$ spectrum.

TABLE IV. Naphthalene dimer: computed ($T_n \leftarrow T_1$) absorption spectrum.[a,b]

Monomer		Dimer		Eclipsed dimer, $R=3.6$ Å				V-shaped dimer, $R=4.2$ Å			
S_n	E(eV)	f	State label	T_n	E(eV)	f	**M** vector (a.u.)	T_n	E(eV)	f	**M** vector (a.u.)
$T_1(T^{00})$	0.00	⋯	σ_1	T_1	0.00	⋯	⋯	T_1	0.00	⋯	⋯
			γ_1	T_2	0.09	0.00	0.10,*y*	T_2	0.07	0.00	0.09,*y*
			δ_1	T_{13}	3.21	0.10	1.14,*y*	T_{13}	3.29	0.11	1.14,*y*
			ρ_1	T_{14}	3.31	⋯	⋯	T_{14}	3.41	0.00	0.20,*z*
$T_2(T^{02+})$	1.15	0.00	σ_2	T_3	1.15	0.00	0.26,*x*	T_3	1.15	0.00	0.27,*x*
			γ_2	T_4	1.23	⋯	⋯	T_4	1.20	⋯	⋯
$T_3(T^{01+})$	1.69	⋯	σ_3	T_5	1.59	⋯	⋯	T_5	1.64	0.00	0.01,*x*
			γ_3	T_6	1.71	⋯	⋯	T_6	1.68	⋯	⋯
			δ_3	T_{24}	4.05	⋯	⋯	T_{25}	4.23	⋯	⋯
			ρ_3	T_{25}	4.17	⋯	⋯	T_{27}	4.27	0.00	0.11,*x*
T_4	2.15	⋯	σ_4	T_7	2.06	⋯	⋯	T_7	2.14	0.00	0.06,*z*
			γ_4	T_8	2.18	0.00	0.03,*y*	T_8	2.17	0.00	0.04,*y*
$T_5(T^{03+})$	2.28	0.01	σ_5	T_9	2.22	0.01	0.37,*z*	T_9	2.22	0.01	0.36,*z*
			γ_5	T_{11}	2.30	⋯	⋯	T_{10}	2.28	0.00	0.03,*y*
$T_8(T^{12+})$	3.63	0.02	σ_8	T_{17}	3.60	0.03	0.61,*z*	T_{17}	3.67	0.03	0.59,*z*
			γ_8	T_{18}	3.70	⋯	⋯	T_{18}	3.72	0.00	0.03,*y*
$T_{11}(T^{02-})$	4.29	0.40	σ_{11}	T_{23}	3.98	0.39	2.00,*x*	T_{23}	4.02	0.39	2.00,*x*
			γ_{11}	T_{27}	4.22	⋯	⋯	T_{24}	4.19	⋯	⋯
$T_{23}(T^{03-})$	5.74	0.34	σ_{23}	T_{51}	5.35	0.30	1.50,*z*	T_{53}	5.58	0.26	1.37,*z*
			γ_{23}	T_{56}	5.59	⋯	⋯	T_{56}	5.71	0.01	0.32,*y*

[a]All results, including T_n numbering, are from INDO/S calculations. The oscillator strength f is for the transition from the lowest triplet (T_1) state. Transition moment directions are given by axis, where x is the long axis of each monomer and y is the intermonomer axis.

[b]Energies listed are relative to $E(T_1)$ in each case. Computed values of $E(T_1)-E(S_0)$ in each case are: 1.43 eV (monomer), 1.41 eV (eclipsed dimer), 1.45 eV (V-shaped dimer).

Note the appearance of the charge-transfer band $\delta_1 \leftarrow \sigma_1$ ($^3\delta^{00} \leftarrow {}^3\sigma^{00}$), polarized along the intermonomer axis. This band has intensity because the upper and lower states are both of mixed exciton resonance/charge resonance character. The intensity of this band is extremely sensitive to intermonomer distance, which we demonstrate in Fig. 8. For this figure, we recomputed the T-T spectrum of eclipsed dimer at three other values of R, and plotted the results using Gaussian line shapes. The intensity of the CT band doubles for a mere 0.2 Å reduction in R. The other band appearing in the plotted range is the $\sigma_{11} \leftarrow \sigma_1$ ($^3\sigma^{02-} \leftarrow {}^3\sigma^{00}$) band.

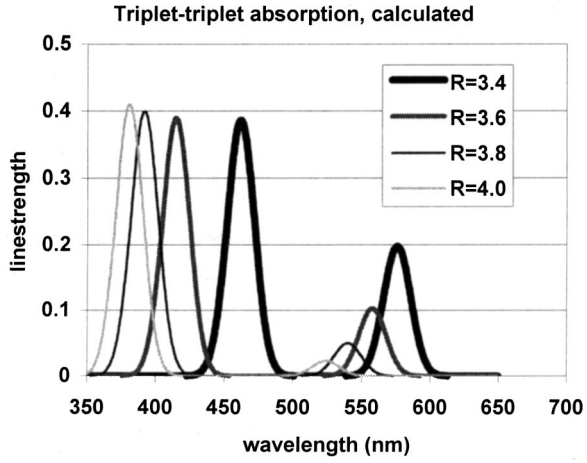

FIG. 8. The predicted $T_n \leftarrow T_1$ absorption spectrum of eclipsed naphthalene dimer, computed at four values of R. Results are from INDO/S calculations, with the poor transition energy predictions reduced by 2.4 eV (before conversion to wavelength) to mimic reality.

Hence, the most substantial changes to the naphthalene T-T absorption spectrum upon dimerization should be a red shift of the $T^{02-} \leftarrow T^{00}$ band (due to splitting of T^{02-} into $^3\sigma^{02-}$ and $^3\gamma^{02-}$) and the appearance of the $^3\delta^{00} \leftarrow {}^3\sigma^{00}$ charge-transfer band at lower energy.

We also computed the eclipsed dimer $S_n \leftarrow {}^1\sigma^{00}$ spectrum at $R=3.6$ and 3.8 Å, although we do not tabulate the results. This spectrum differs from the $T_n \leftarrow T_1$ spectrum of Fig. 8 in two major ways: (i) the two major bands, $\delta^{00} \leftarrow \sigma^{00}$ and $\sigma^{02-} \leftarrow \sigma^{00}$ are at longer wavelengths, since $E(S_1) > E(T_1)$, and (ii) the T-T $^3\sigma^{02-} \leftarrow {}^3\sigma^{00}$ band is split into two. Another significant difference is that the bright $^1\delta^{00} \leftarrow {}^1\sigma^{00}$ and normally dark $^1\gamma^{00} \leftarrow {}^1\sigma^{00}$ transitions are nearly equal in energy at $R=3$ Å, which allows a route to populating the dissociative $^1\gamma^{00}$ state via infrared absorption of the $^1\sigma^{00}$ excimer.

E. Analysis of monomer $S_0 \leftarrow T_1$ transitions

Before we address $S_0 \leftarrow T_1$ transitions of model naphthalene dimers, we wish to review and comment on the $S_0 \leftarrow T_1$ transitions of naphthalene monomer.

For the phosphorescence of naphthalene, experimental results were quantitatively reproduced by Knuts, Ågren, and Minaev,[28] who used linear response theory to compute a radiative lifetime of about 1 min, with decay rate ratios of $k_x:k_y:k_z = 140:1:0$ indicating overwhelmingly out-of-plane polarization. To investigate which spin-orbit channels are active in this process, we computed spin-orbit coupling integrals with twenty intermediate states, and found no term bigger than 7 cm^{-1}. This is unlike the formaldehyde case where

TABLE V. Naphthalene T_1 phosphorescence: intermediate state table.[a]

Intermediate type	Symmetry	# of channels	$\langle H_{SO}\rangle$, cm^{-1}	$\langle E\rangle$, eV	$\langle M\rangle$,[b] a.u.	$\langle A\rangle$, a.u./eV
$T(\pi\rightarrow\pi^*)$	$^3B_{3g}$	6	0.4	7	0.4_y	0.0571
$T(\sigma\rightarrow\pi^*)$	$^3B_{2g}$	25	3	12	0.1_x	0.0083
	$^3B_{1g}$	23	3	12	0	0
$T(\pi\rightarrow\sigma^*)$	$^3B_{2g}$	25	3	12	0.1_x	0.0083
	$^3B_{1g}$	23	3	12	0	0
$T(\sigma\rightarrow\sigma^*)$	$^3B_{3g}$	92	3	20	0.03_y	0.0015
$S(\pi\rightarrow\pi^*)$	$^1B_{2u}$	4	0.4	7	0.4_y	0.1000
$S(\sigma\rightarrow\pi^*)$	$^1B_{3u}$	5	3	12	0.1_x	0.0111
	^1A_u	4	3	12	0	0
$S(\pi\rightarrow\sigma^*)$	$^1B_{3u}$	5	3	12	0.1_x	0.0111
	^1A_u	4	3	12	0	0
$S(\pi\pi\rightarrow\pi^*\pi^*)$	$^1B_{2u}$	10	0.4	8	0	0
$S(\sigma\pi\rightarrow\pi^*\pi^*)$	$^1B_{3u}$	46	3	18	0	0
	^1A_u	40	3	18	0	0
$S(\pi\pi\rightarrow\pi^*\sigma^*)$	$^1B_{3u}$	46	3	18	0	0
	^1A_u	40	3	18	0	0
$S(\sigma\pi\rightarrow\pi^*\sigma^*)$	$^1B_{2u}$	184	3	23	0	0

[a]These data are used for evaluation of Eq. (8), where $\langle A\rangle$ is $\langle M\rangle/[\langle E\rangle - E(T_1)]$ for intermediate singlet states, and $\langle M\rangle/\langle E\rangle$ for intermediate triplet states. The choices for the expectation values are based on exploratory calculations; see text for details.

[b]The x and y polarization directions correspond to the out-of-plane and long axes, respectively.

there were terms on the order of 50 cm^{-1},[9] but similar to the ethene case where the two largest terms are roughly 20 and 10 cm^{-1}.[29] Hence, in the expression for the radiative transition dipole moment [Eq. (5)], the summations display rather slow convergence, and many spin-orbit channels will contribute. However, we can use a channel-counting scheme (Sec. II B) to account for the observed polarization direction.

Since the symmetries (in our axis convention) for the S_0 and T_1 states are A_g and B_{1u}, and since the spatial-symmetry components of H_{SO} have symmetry B_{1g}, B_{2g}, or B_{3g}, the direct spin-orbit channel $\langle S_0|H_{SO}|T_1\rangle$ is forbidden. For the intermediary channels, the allowed singlet intermediate states for $\langle S_n|H_{SO}|T_1\rangle$ are A_u, B_{2u}, and B_{3u}, and the allowed triplet intermediate states for $\langle S_0|H_{SO}|T_n\rangle$ are B_{1g}, B_{2g}, and B_{3g}. Our 20 computed examples of these terms suggests that coupling strength comes in just two classes for this molecule: a weak coupling to $\sigma\rightarrow\sigma^*$, $\sigma\rightarrow\pi^*$ and $\pi\rightarrow\sigma^*$ states (range 0.2–6.6 cm^{-1}), and a very weak coupling to $\pi\rightarrow\pi^*$ states (range 0.3–1.4 cm^{-1}). The channel counts and typical coupling values appear in Table V.

For radiative transitions, the allowed singlet states for $\langle S_0|M|S_n\rangle$ transitions are B_{3u}, B_{2u}, and B_{1u} (for x, y, and z polarization, respectively), and the allowed triplet states are B_{2g}, B_{3g}, and A_g for $\langle T_n|M|T_1\rangle$ transitions. Comparing this with the allowed spin-orbit channels, we see connections only for x-polarized phosphorescence (B_{3u} singlets and B_{2g} triplets) and y-polarized phosphorescence (B_{2u} singlets and B_{3g} triplets). We next want the A coefficients in Eq. (8), and the crucial quantities are the transition moments and energies to the intermediate states. These quantities can vary tremendously, and therefore ''best guesses'' as to a crude average value are required. Our choices, based on INDO/S and Rubio *et al.*,[15] also appear in Table V. Using the data of Table V for each polarization direction, we obtain $W_x^2{:}W_y^2{:}W_z^2$ ratios of 5:1:0, which qualitatively agree with the old 10:1:1 experimental estimates of Sixl and Schwoerer,[30] and the 140:1:0 ratios of the linear response calculation.[28]

For nonradiative transitions, we can employ a similar procedure. We have already counted the spin-orbit channels. Allowed $\langle S_0|\partial/\partial Q_k|S_n\rangle$ couplings to valid S_n spin-orbit channels require Q_k (normal mode) symmetries of B_{3u}, A_u, or B_{2u}. Allowed $\langle T_n|\partial/\partial Q_k|T_1\rangle$ couplings to valid T_n spin-orbit channels require the same three Q_k symmetries. To determine the A values of Eq. (8), one also needs to consider intermediate state energies, number of normal mode subchannels of each symmetry, and magnitudes of the Q_k-dependent terms C_k and $\langle\partial/\partial Q_k\rangle$. The Q_k-dependent quantities are difficult to estimate in a general way, and somewhat too far removed from the crude purposes of the present study. In addition, the approximations inherent in Eqs. (6) and (7) may be somewhat crude as well. We will settle for presenting a set of choices which reproduces experimental rate ratios, and leave the verification of the chosen ''best guess'' values for future research. We use Eq. (7), set all C_k equal to a constant, and use the data presented in Table VI. From this data, we obtain $W_x^2{:}W_y^2{:}W_z^2$ ratios of 1:14:11 for the three T_1 components, which mimics the experimental ratios of 1:12:7.[30]

F. Analysis of dimer $S_0\leftarrow T_1$ transitions

We now wish to apply this channel-counting scheme for triplet-state decay for various orientations of naphthalene dimer, in hopes of shedding some light on possible orientation dependence of the decay rates. Before we applied the channel-counting scheme, however, we needed some calculations to learn more about spin-orbit coupling in dimers.

To understand the dimer orientation effects upon spin-orbit coupling, we computed the $\langle S_0|H_{SO}|T_1\rangle$ coupling integral for various orientations and R values of the simpler

TABLE VI. Naphthalene T_1 nonradiative decay: intermediate state table.[a]

Intermediate type	Symmetry	# of channels	$\langle H_{SO}\rangle$, cm^{-1}	$\langle E\rangle$, eV	$N(Q_k)$	$\langle \partial/\partial Q_k\rangle$, $Å^{-1}$	$\langle A\rangle$, $Å^{-1}$/eV
$T(\pi\rightarrow\pi^*)$	$^3B_{3g}$	6	0.4	7	8	1	1.143
$T(\sigma\rightarrow\pi^*)$	$^3B_{2g}$	25	3	12	4	1	0.333
	$^3B_{1g}$	23	3	12	4	1	0.333
$T(\pi\rightarrow\sigma^*)$	$^3B_{2g}$	25	3	12	4	1	0.333
	$^3B_{1g}$	23	3	12	4	1	0.333
$T(\sigma\rightarrow\sigma^*)$	$^3B_{3g}$	92	3	20	8	0.1	0.040
$S(\pi\rightarrow\pi^*)$	$^1B_{2u}$	4	0.4	7	8	1	2.000
$S(\sigma\rightarrow\pi^*)$	$^1B_{3u}$	5	3	12	4	1	0.444
	^1A_u	4	3	12	4	1	0.444
$S(\pi\rightarrow\sigma^*)$	$^1B_{3u}$	5	3	12	4	1	0.444
	^1A_u	4	3	12	4	0	0.444
$S(\pi\pi\rightarrow\pi^*\pi^*)$	$^1B_{2u}$	10	0.4	8	8	0	0
$S(\sigma\pi\rightarrow\pi^*\pi^*)$	$^1B_{3u}$	46	3	18	4	0	0
	^1A_u	40	3	18	4	0	0
$S(\pi\pi\rightarrow\pi^*\sigma^*)$	$^1B_{3u}$	46	3	18	4	0	0
	^1A_u	40	3	18	4	0	0
$S(\sigma\pi\rightarrow\pi^*\sigma^*)$	$^1B_{2u}$	184	3	23	8	0	0

[a]These data are used for evaluation of Eq. (8), where $\langle A\rangle$ is $C_k N(Q_k)\langle\partial/\partial Q_k\rangle/[\langle E\rangle - E(T_1)]$ for intermediate singlet states, and $C_k N(Q_k)\langle\partial/\partial Q_k\rangle/\langle E\rangle$ for intermediate triplet states. The choices for the expectation values are based on exploratory calculations; see text for details.

$(C_2H_4)_2$ system. It was difficult to detect any orientation dependence of this coupling, because of the strong exponential decay of the coupling with increasing R, but the orientation dependence did seem rather small when comparing values at realistic values of R.

We turned to the naphthalene dimer, and began to compute spin-orbit couplings of the T_1 state to several intermediate $\pi\rightarrow\pi^*$ S_n states. We soon made the following important discovery: there are *no valid spin-orbit channels* which contribute to T_1 radiative decay in the eclipsed and conrotated orientations. The reason for this is inversion symmetry. In naphthalene dimers that possess a center of inversion, the S_0 and T_1 states are of gerade symmetry. Since the spatial parts of the H_{SO} operator are also gerade, only gerade intermediate states can be allowed spin-orbit channels. However, gerade intermediates cannot contribute to T_1 phosphorescence because the axial components of the transition dipole operator **M** are of ungerade symmetry, which causes their S_0-S_n or T_n-T_1 transitions to be forbidden. Therefore, radiative decay of the T_1 state of naphthalene dimer must be significantly more rapid in orientations which do not possess inversion symmetry, such as the disrotated and *T*-shaped orientations.

Understanding this, we computed spin-orbit couplings of the T_1 state to six intermediate $\pi\rightarrow\pi^*$ S_n states ($^1\gamma_1$, $^1\delta_1$, $^1\sigma_2$, $^1\gamma_2$, $^1\gamma_4$, $^1\delta_4$), but for only the 20°-disrotated (V-shaped) dimer at $R=4.4$ Å. The values, which appear in Table VII, are all less than 0.5 cm^{-1}; these small values are understandable since they are all zero when the dimer is not disrotated. Table VII also lists data garnered from Tables III and IV pertinent to phosphorescence [Eq. (8)]. Note that these A values are larger than those in Table V, partly because INDO/S has overestimated the *S-S* transition moments.[17]

We also calculated the direct spin-orbit coupling of T_1 to S_0, $\langle S_0|H_{SO}|T_1\rangle$, for the free dimer in eclipsed ($R=3.8$) and V-shaped ($R=4.4$) orientations [$\langle H_{SO}\rangle=0.3\,cm^{-1}$ in both cases]. We also computed this integral for realistic structures of two covalently bound naphthalene dimers. The Agosta dimer[31] is a 55°-disrotated form with $R=4.7$ Å, for which $\langle H_{SO}\rangle=1.0\,cm^{-1}$. The DBB dimer, *syn*-[4.4][1,5]-naphthalenophane,[32] is an eclipsed dimer with two butyl bridges connecting the 1 and 5 positions, with $R=3.0$ Å between the 1 and 5 positions and $R=3.4$ Å between the 4 and 8 positions, for which $\langle H_{SO}\rangle=1.0\,cm^{-1}$ as well. These values are sufficiently small that we expect radiative and nonradiative decay in these systems to be dominated by cumulative contributions from intermediate states.

Next we applied the channel-counting scheme for T_1 radiative and nonradiative decay, for several orientations of naphthalene dimer: D_{2h} eclipsed, C_{2v} disrotated, C_{2h} conrotated, C_{2h} puckered (where the monomers have been bent closer at the 1 and 5 positions, to mimic the DBB dimer

TABLE VII. V-shaped dimer: computed spin-orbit couplings, and other data relevant for radiative T_1 decay.

S_n	Symmetry	$\langle S_n\|H_{so}\|T_1\rangle$,[a] cm^{-1}	$E(S_n)-E(T_1)$,[b] eV	$M(S_n-S_0)$,[c] a.u.	A,[d] a.u./eV
$^1\gamma_1(^1\gamma^{01+})$	$^1B_1$	0.4,*z*	0.8	0.35,*x*	0.4
$^1\delta_1(^1\delta^{01+})$	$^1B_1$	0.0	2.6	3.53,*x*	1.4
$^1\sigma_2(^1\sigma^{00})$	$^1B_2$	0 by symmetry	1.1	0.88,*y*	0.8
$^1\gamma_2(^1\gamma^{00})$	$^1A_1$	0.0	1.3	1.75,*z*	1.3
$^1\gamma_4(^1\gamma^{01-})$	$^1B_1$	−0.1,*z*	2.8	3.55,*x*	1.3
$^1\delta_4(^1\delta^{01-})$	$^1A_2$	−0.1,*z*	2.9	0.37,*x*	0.1

[a]Spin-orbit couplings are from CASSCF(8-in-8)/6-31G calculations, $R=4.4$ Å, 20° disrotation.

[b]Energies obtained from Table III, subtracting 3 eV for the energy of the dimer T_1 state.

[c]Transition moments are from Table III; directions are given by axis, where *x* is the long axis of each monomer and *y* is the intermonomer axis.

[d]The *A* parameter is for Eq. (8); see footnote a of Table V.

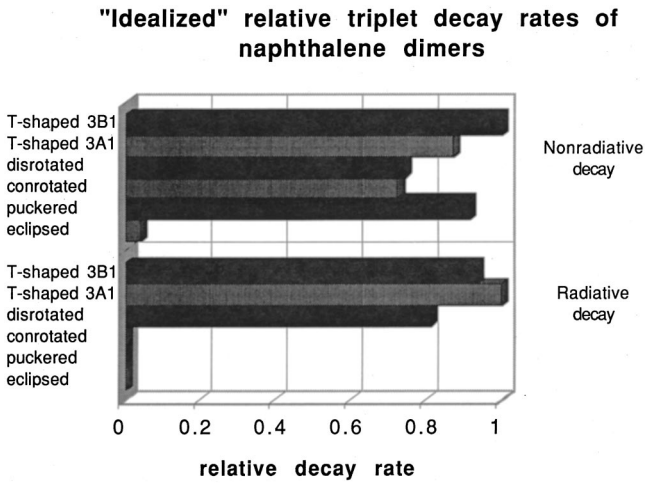

FIG. 9. ''Idealized'' T_1 state decay rates, relative to the fastest rate in each of the two cases. Results are from our application of a spin-orbit-channel-counting scheme; see text.

above), and C_{2v} T-shaped. For the T-shaped case we applied the scheme for both the $^3B_1$ and $^3A_1$ states because they are both candidates for the actual T_1 state (see Fig. 5). The channel-counting and Eq. (8) evaluations were performed on computer with roughly 500 lines of FORTRAN code. Unfortunately, values for $\langle H_{\mathrm{SO}}\rangle$, $\langle E\rangle$, $\langle M\rangle$, and $\langle \partial/\partial Q_k\rangle$ are difficult to assess for high-lying states of these dimers, and hence we have kept them fixed at their monomer values. Admittedly, this is a poor approximation. However, this choice has the benefit of placing the effect of orientation solely in the number of spin-orbit channels and the number $N(Q_k)$ of corresponding allowed normal modes. Our ''idealized'' results, therefore, will be more reflective of the number of contributing channels for each orientation, rather than the actual relative rates.

The end result of these calculations are *W*-values [Eq. (8)] for each of the three triplet components, which we square to obtain component decay rates, and then average to obtain the high-temperature T_1 decay rate. The results appear in Fig. 9, expressed as decay rates relative to those of the other orientations, for both the radiative and non-radiative cases. For T_1 radiative decay, we see the result (stated earlier) that there is no allowed phosphorescence from dimers having a center of inversion symmetry. As for T_1 nonradiative decay, the D_{2h} form decays more slowly than the other forms due to much fewer allowed spin-orbit channels, while amongst the lower-symmetry forms there is only a 25% variation in the predicted idealized decay rate, as based on available spin-orbit channels. Note, however, that for small conrotations, disrotations, or puckerings, the nonradiative decay rates of these three forms must be near the eclipsed-dimer rate, so that the effect of their extra allowed channels is important only for significant deviations from the D_{2h} eclipsed form.

V. COMPARISON WITH EXPERIMENT

The various computational results of Sec. IV, other than Figs. 4–7, are largely qualitative in accuracy because of the approximations involved. In addition to this, the comparison of monomer results to free dimer results is only the first step in modeling the results of covalently bonded dimers, which also contain ring puckering and other effects. However, this first step is the most important step in understanding the spectroscopy and the photophysics of naphthalene dimers, either free ones or covalently bonded ones, and these results already provide important predictions that can be compared with the experimental results. Among these are:

(1) The triplet excimers of naphthalene are predicted to be more stable than the van der Waals ground state, but only in a face-to-face monomer arrangement, in which their binding energies can be enhanced by CT interaction (Sec. IV B).

(2) Whereas the singlet excimer is stabilized by exciton resonance as well as CT interaction, the triplet excimer is stabilized mostly by CT interaction. As such, the binding is significantly smaller for the triplet excimer $^3\sigma^{00}$ as compared to the singlet excimer $^1\sigma^{00}$ (Sec. IV B).

(3) Unlike the singlet excimer, which clearly prefers an eclipsed (sandwich-pair) geometry due to stabilization by exciton resonance as well as charge resonance, the triplet excimer may adopt other conformations as well (Sec. IV B).

(4) For the triplet excimer of eclipsed geometry, the $^3\sigma$-$^3\gamma$ splitting is nontrivial, commensurate with the splitting of the weakly absorbing ^1L_b state (Sec. IV B).

(5) $S_1(^1\sigma^{00})$-S_0 transitions are forbidden for eclipsed dimers, and therefore S_1 states should have relatively long lifetimes with respect to fluorescence (Sec. IV C).

(6) In $T_n \leftarrow T_1$ absorption, the most noteworthy spectroscopic consequence of intermolecular excimeric interactions in the dimer is a red shift of the monomer absorption bands and the appearance of an interchromophore CT band at lower energy (Sec. IV D).

(7) The interchromophore $\delta \leftarrow \sigma$ CT absorption, whose intensity strongly increases with decreasing separation, is a very useful probe of the interchromophore interaction in the excited state leading to excimer formation (Sec. IV D).

(8) In an eclipsed dimer, the higher energy exciton component of each dimeric state, i.e., the γ state, is repulsive (Sec. IV B). Photodecomposition or fragmentation of the stable excimer can therefore occur via these repulsive excited states, particularly if one lies near an absorbing state (Sec. IV D).

(9) The radiative transition probabilities are very small for triplet excimers with inversion symmetry. The T_1 and S_0 states are both of gerade symmetry for dimers with a center of symmetry, which makes the phosphorescence doubly forbidden, i.e., spatially as well as spinwise (Sec. IV F).

Results 1–4 have direct relevance to the questions of stability and preferred geometry of naphthalene triplet excimer. Since the T_1 state of the dimer is stabilized by CT (in addition to London dispersion forces), the eclipsed and crossed orientations may be preferred over other orientations for the triplet excimer because they allow closer proximity for the two monomers. However, there is considerable uncertainty in the computed binding energy of the T_1 state. Indeed, the 1970 experiments by Chandross and Dempster,[33] which produced face-to-face dimers with monomerlike triplet states, suggest that there may not be significant enhancement of the T_1 binding energy in the eclipsed conformation.

Result 5 likely explains the excimer emission lifetimes of Yanagidate *et al.*,[32] who noted longer S_1 radiative lifetimes in eclipsed [4.4]naphthalenophanes than in tilted [2.4]naphthalenophanes.

Result 6 is confirmed by experimental triplet-triplet absorption spectra of covalently bonded dimers[34–36] which compare very well with our smallest-R prediction of Fig. 8. The $T_n \leftarrow T_1$ absorption spectrum of the naphthalene monomer at about 420 nm shifts to the red upon dimerization, and a new longer-wavelength absorption at about 600 nm appears in the dimer spectra. The assignment of the 600 nm absorption to the interchromophore $^3\delta \leftarrow ^3\sigma$ CT transition was first made by Ishikawa *et al.*,[34] and is supported by the fact that the corresponding singlet-singlet $^1\delta \leftarrow ^1\sigma$ transition occurs at lower energy (~700 nm),[37,38] since this is consistent with the near degeneracy of the CT singlet and triplet states ($^1\delta$ and $^3\delta$), and the higher energy of the $^1\sigma$ state relative to $^3\sigma$. The difference in the transition energies is consistent with the $^1\sigma$-$^3\sigma$ electronic energy gap.

Result 7 is supported by the observation that covalently bonded dimers of naphthalene exhibiting excimer phosphorescence all display the $^3\delta \leftarrow ^3\sigma$ CT absorption in the 500–650 nm region, independent of the relative orientation of the two naphthalenes.[36] The intermoiety CT absorption band has also been observed in the covalently bonded dimers of pyrene[34] and biphenyl.[39]

Result 8 explains the experimental results of Saigusa, Sun, and Lim,[37,38] who observed photodissociation of the singlet excimer at near-infrared wavelengths. The bright $^1\delta^{00}$ state of predominately CT character is the likely upper state of the absorption, which then interconverts to the dissociative $^1\gamma^{00}$ state, although it may just lend intensity to the normally dark $^1\gamma^{00}$ state and allow it to be accessed directly. The assignment of a CT state as the infrared-absorbing state was made by Katoh *et al.*[40] for singlet excimer of naphthalene and other aromatic hydrocarbons, based on the approximate correlation between the transition energy and the difference between the estimated energy of the CT state and the energy of the excimer singlet state.

Result 9 might be contributing to the reduced phosphorescence intensity seen in work on naphthalenophanes by Schweitzer *et al.*[41] It may also account for the interesting observation of Shizuka and co-workers[35] that syn-[3.4](1,5)naphthalenophane does not apparently phosphoresce in rigid glass at 77 K, despite the fact that the compound displays the intermoiety CT absorption characteristic of a naphthalene triplet excimer. It is possible that earlier reports of monomeric phosphorescence from a sandwich dimer and naphthalenophanes are related to distortion to noncentrosymmetric conformations or interplanar separations too large for an effective intermoiety interaction leading to excimer formation. These experimental results should be reanalyzed again, however, once the effects of the interchromophore covalent connections are studied.

VI. CONCLUSIONS

We have applied standard quantum chemistry techniques in a nonstandard way to obtain much useful information on the excited states of naphthalene dimer. We have been able to provide plots correlating electronic state energies of the dimers, at various monomer orientations and values of R, for the first time. We have also correlated the electronic excitations of the dimeric species to those of the monomers. These results should be valuable resources for understanding experimental results of the past, present, and future.

Many results are relevant to triplet excimers. Unlike the singlet excimer, which is bound by both exciton resonance and CT resonance, triplet excimers should be bound only by CT resonance. As a result, they are predicted to be less stable than their singlet excimer counterparts, and more prone to adopting other orientations, rather like the ground state dimer. Eclipsed or crossed orientations are expected to be preferred, however, since these afford a closer approach for stronger CT benefits. The exciton splitting of the $^3\sigma$ and $^3\gamma$ states is nontrivial at bonding distances, commensurate with the weak exciton splitting of the ^1L_b state.

The appearance of an additional CT band in $T_n \leftarrow T_1$ and $S_n \leftarrow S_1$ spectra is predicted here, and the actual state assignment is made here for several experimental spectra of covalently bonded naphthalene dimers. The assignment of the $^3\delta^{00} \leftarrow ^3\sigma^{00}$ CT band verifies that interchromophore interaction is quite likely in the $T_1(^3\sigma^{00})$ state. The $^1\delta^{00} \leftarrow ^1\sigma^{00}$ CT band is shown to provide a route to the dissociative $^1\gamma^{00}$ state via IR absorption of the singlet excimer, because the $^1\delta^{00}$ and $^1\gamma^{00}$ states are so close in energy at singlet excimer geometries.

A state-counting scheme has been presented for T_1 radiative and nonradiative decay, which seems to account for T_1 radiative-decay polarization results and T_1 nonradiative-decay triplet-sublevel results of naphthalene monomer. We applied this scheme to T_1 decay of the dimers, and found a strong orientation dependence on radiative decay, but not for nonradiative decay. In particular, T_1 phosphorescence is forbidden for naphthalene dimers with a center of inversion, such as eclipsed, conrotated, and symmetrically-puckered dimers.

ACKNOWLEDGMENTS

This work was supported by the Division of Chemical Sciences, Office of the Basic Energy Sciences, United States Department of Energy. One of us (A.E.) would like to thank M. Lee for office space and kind hospitality during most of the project duration.

[1] G. D. Scholes and K. P. Ghiggino, J. Phys. Chem. **98**, 4580 (1994).
[2] R. G. Sadygov and E. C. Lim, Chem. Phys. Lett. **225**, 441 (1994).
[3] M. S. Gudipati, J. Phys. Chem. **98**, 9750 (1994).
[4] S. Tretiak, W. M. Zhang, V. Chernyak, and S. Mukamel, Proc. Natl. Acad. Sci. U.S.A. **96**, 13003 (1999).
[5] E. G. McRae and M. Kasha, in *Physical Processes in Radiation Biology* (Academic, New York, 1964).
[6] A. K. Chandra and E. C. Lim, J. Chem. Phys. **48**, 2589 (1967).
[7] A. Messiah, *Quantum Mechanics* (North-Holland, Amsterdam, 1962), Vol. 2, p. 736.
[8] B. R. Henry and W. Siebrand, J. Chem. Phys. **54**, 1072 (1971).
[9] S. R. Langhoff and E. R. Davidson, J. Chem. Phys. **64**, 4699 (1976).
[10] GAUSSIAN 98, M. J. Frisch, G. W. Trucks, H. B. Schlegel, G. E. Scuseria, M. A. Robb, J. R. Cheeseman, V. G. Zakrzewski, J. A. Montgomery, R. E. Stratmann, J. C. Burant, S. Dapprich, J. M. Millam, A. D. Daniels, K. N. Kudin, M. C. Strain, O. Farkas, J. Tomasi, V. Barone, M. Cossi, R. Cammi, B. Mennucci, C. Pomelli, C. Adamo, S. Clifford, J. Ochterski, G.

A. Petersson, P. Y. Ayala, Q. Cui, K. Morokuma, D. K. Malick, A. D. Rabuck, K. Raghavachari, J. B. Foresman, J. Cioslowski, J. V. Ortiz, B. B. Stefanov, G. Liu, A. Liashenko, P. Piskorz, I. Komaromi, R. Gomperts, R. L. Martin, D. J. Fox, T. Keith, M. A. Al-Laham, C. Y. Peng, A. Nanayakkara, C. Gonzalez, M. Challacombe, P. M. W. Gill, B. G. Johnson, and J. A. Pople (Gaussian, Inc., Pittsburgh, PA, 1998).
[11] J. Ridley and M. Zerner, Theor. Chim. Acta **32**, 111 (1973); **42**, 223 (1976).
[12] J. B. Foresman, M. Head-Gordon, J. A. Pople, and M. J. Frisch, J. Phys. Chem. **96**, 135 (1992).
[13] C. Moller and M. S. Plesset, Phys. Rev. **46**, 618 (1934).
[14] S. Koseki, M. W. Schmidt, and M. S. Gordon, J. Phys. Chem. **96**, 10768 (1992).
[15] M. Rubio, M. Merchan, E. Orti, and B. O. Roos, Chem. Phys. **179**, 395 (1994).
[16] K. L. Bak, H. Koch, J. Oddershede, O. Christiansen, and S. P. A. Sauer, J. Chem. Phys. **112**, 4173 (2000).
[17] M. A. Thompson and M. C. Zerner, J. Am. Chem. Soc. **113**, 8210 (1991).
[18] E. A. Chandross, J. Ferguson, and E. G. McRae, J. Chem. Phys. **45**, 3546 (1966).
[19] B. T. Lim and E. C. Lim, J. Chem. Phys. **78**, 5262 (1983).
[20] E. C. Lim, Acc. Chem. Res. **20**, 8 (1987).
[21] C. Gonzalez and E. C. Lim, J. Phys. Chem. A **104**, 2953 (2000).
[22] R. L. Jaffe and G. D. Smith, J. Chem. Phys. **105**, 2780 (1996).
[23] P. Hobza, H. L. Selzle, and E. W. Schlag, J. Phys. Chem. **100**, 18790 (1996).
[24] V. Spirko, O. Engkvist, P. Soldan, H. L. Selzle, E. W. Schlag, and P. Hobza, J. Chem. Phys. **111**, 572 (1999).
[25] M. C. R. Cockett, H. Ozeki, K. Okuyama, and K. Kimura, J. Chem. Phys. **98**, 7763 (1993).
[26] S. F. Boys and F. Bernardi, Mol. Phys. **19**, 553 (1970).
[27] A. L. L. East, P. Cid-Aguero, H. Liu, R. H. Judge, and E. C. Lim, J. Phys. Chem. A **104**, 1456 (2000).
[28] S. Knuts, H. Ågren, and B. F. Minaev, J. Mol. Struct.: THEOCHEM **311**, 185 (1994).
[29] H. Ågren, O. Vahtras, and B. Minaev, Adv. Quantum Chem. **27**, 71 (1996).
[30] H. Sixl and M. Schwoerer, Chem. Phys. Lett. **6**, 21 (1970).
[31] W. C. Agosta, J. Am. Chem. Soc. **89**, 3505 (1967).
[32] M. Yanagidate, K. Takayama, M. Takeuchi, J. Nishimura, and H. Shizuka, J. Phys. Chem. **97**, 8881 (1993).
[33] E. A. Chandross and C. J. Dempster, J. Am. Chem. Soc. **92**, 704 (1970).
[34] S. Ishikawa, J. Nakamura, S. Iwata, M. Sumitani, S. Nagakura, Y. Sakata, and S. Misumi, Bull. Chem. Soc. Jpn. **52**, 1346 (1979).
[35] M. Yamaji, H. Tsukada, J. Nishimura, and H. Shizuka, private communication.
[36] X. Wang, W. G. Kofron, S. Kong, C. S. Rajesh, D. A. Modarelli, and E.C. Lim, J. Phys. Chem. A **104**, 1461 (2000).
[37] H. Saigusa, S. Sun, and E. C. Lim, J. Phys. Chem. **96**, 10099 (1992).
[38] S. Sun, H. Saigusa, and E. C. Lim, J. Phys. Chem. **97**, 11635 (1993).
[39] M. Yamaji (private communication).
[40] R. Katoh, E. Katoh, N. Nakashima, M. Yuuki, and M. Kotani, J. Phys. Chem. A **101**, 7725 (1997).
[41] D. Schweitzer, J. P. Colpa, J. Behnke, K. H. Hausser, M. Haenel, and H. A. Staab, Chem. Phys. **11**, 373 (1975).